Radio Frequency Fingerprint Identification Technology Considering Strong Interference of Electromagnetic Noise

Yang Kong*, Rongwei Dong
School of Intelligent Manufacturing, Yancheng Polytechnic College, Yancheng 224001, China
E-mail: gchio1982@126.com
*Corresponding author

Keywords: electromagnetic noise, radio frequency fingerprint recognition, attention mechanism, lightweight processing, signal-to-noise ratio

Received: May 7, 2024

To improve the anti-interference ability of RF fingerprint identification technology, the study adopts the improved sketch algorithm to screen the raw data. The extraction of important features and high-frequency signals from raw data is achieved through a series of steps, including partitioning, calculation of local correlation, data filtering, and aggregation. This process is facilitated by the use of a growing self-organizing model, which labels the data. Next, a residual network model with channel attention mechanism is used for feature extraction and classification, and a customized nonlinear activation function and dynamic threshold noise reduction algorithm are introduced. This model employs a two-dimensional convolutional kernel to safeguard the phase feature information of the I/Q data, and integrates a channel attention mechanism and a dynamic threshold function. The results demonstrated that the sketch algorithm was capable of effectively controlling the estimation error of high-frequency sub-signals to within 14%. The differences in classification clusters of K-means and growing self-organizing model clustering algorithms were 0.2691 and 0.2639, with time overheads of 8.6 s and 2.3 s. The residual network model based on the channel-attention mechanism exhibited a recognition accuracy of 98.2%, which was higher than that of the other three comparative models when the signal-to-noise ratio was 10 dB. It is shown that the performance performance and robustness of the model can be further improved by optimizing the shape and size of the network using the attention mechanism and adaptive methods. The research and application of this method is of great significance for improving the accuracy and robustness of RF signal fingerprinting.

Povzetek: Študija uporablja izboljšan algoritem za prepoznavanje radijskih frekvenčnih prstnih odtisov, ki vključuje mehanizem pozornosti in algoritme za zmanjševanje šuma, s čimer dosega visoko natančnost prepoznavanja in robustnost v prisotnosti močnega elektromagnetnega šuma.

1 Introduction

Radio frequency fingerprint recognition (RFFR) technology is widely used in identity authentication, access control, network security, and other fields due to the development of radio frequency (RF) technology [1]. This technique utilizes the feature information in the electromagnetic spectrum to convert the electromagnetic field distribution of the object to be recognized into a specific spectral pattern, thus realizing the recognition and tracking of the target object [2]. However, the RFFR technique may be affected by interference factors, such as electromagnetic noise (EMN), in practical applications. These elements may result in security risks and performance degradation, which could have a negative impact on the technique's accuracy and dependability [3]. For example, in strong interference environments, fingerprint features (FPF) may be masked by interference signals, leading to recognition errors [4]. In addition, conventional RFFR techniques require the use of high-power signals for FPF extraction, which may generate electromagnetic radiation pollution and negatively affect the environment [5]. Therefore, how to introduce anti-jamming mechanism in RFFR technique to improve its robustness under strong interference environment has become a common concern in both academia and industry. In order to solve these problems, the research proposes an RFFR technique considering strong interference from EMNs and feature extraction by lightweight processing (LWP) method to improve fingerprint recognition under low power consumption. This study is broken down into four sections. The first section is an overview of the EMN and RFFR research. The second part is to design the new RFFR method and validate it in the third part and the fourth part is to summarize the whole research.

EMN interference signal processing refers to the processing of signals subjected to EMN interference by filtering and noise reduction methods in order to recover their original information or minimize the influence of

the interference. A high-voltage power supply EMN filtering technique for electric vehicle motor drive systems was proposed by Zhai et al. Moreover, by examining the common mode and differential mode interference routes at two crucial frequency sites, 1 MHz and 30 MHz, they were able to ascertain the primary overrun point parameters. The outcomes showed that the approach could accomplish the design goals [6]. For line-polarized waves, Han's team designed a dual-frequency asymmetric transmission supersurface with dual anisotropic metal layers to improve the asymmetric transmission capability and operation bandwidth. The results demonstrated that the method produced asymmetric transmission parameters greater than 0.8 in both operating frequency bands, and derived sub-bandwidths of 1.18% and 21.39%, respectively [7]. Li et al. proposed a Magnetelluric noise suppression method based on deformation pattern decomposition by reducing the fluctuation analysis to select the appropriate decomposition layer. The method improved the accuracy of signal decomposition and the reliability of reconstructed signals by adaptively selecting appropriate orders for different types of disturbances. The results indicated that the denoised data from this method can further enhance the reliability of geoelectric information [8]. Wang et al. researchers designed a radar transmit matrix using a hierarchical approach to transform the original problem into two sub-problems, the transmit design for suppressing the side-flap interference and the target detection signal design under the main-flap interference, respectively. Compared with the existing methods, this method was more flexible to balance the matching loss and spectral compatibility, which could improve the radar target detection performance in interference environment [9]. The Zhang research group utilized the difference between the signaling channel and the residual self-interference channel for resource allocation to suppress residual self-interference and increase system capacity. The method modeled the residual self-interference channel and the user uplink channel as multipath frequency-selective fading channels satisfying a Rayleigh distribution. Experimental results showed that the scheme has effectiveness and provides an effective resource allocation strategy for broadband full-duplex systems [10].

RF identification technology is a subset of automatic identification technology that uses wireless RF to allow non-contact, two-way data communication. It reads and writes to recording media to facilitate data exchange and target identification. Tan's team utilized the spatial correlation between RF and geomagnetic signals to mitigate the effects of sensor noise in order to improve the accuracy of fingerprint identification without explicit manual intervention. Experiments showed that this method can reduce RF and geomagnetic fingerprint identification errors by 40% [11]. Cutts et al. proposed a method for temporal filtering of RF signals that utilizes an edge time-series approach to decompose functional magnetic resonance imaging frames in order to define enhanced recognizability features. The results showed that the method can recognize several different fingerprints by considering both spatial and temporal features [12]. Shi's group proposed a photonic method for incorporating RF self-interference cancellation into in-band full-duplex fiber optic radio systems. Experiments demonstrated that the method can achieve a cancellation depth of greater than 20 dB for orthogonal amplitude modulated signals in a back-to-back scenario [13]. To increase the classification accuracy, Shen's team developed a deep learning-based RFFR scheme that makes use of estimated parameters to fine-tune the deep learning model's predictions. The spectrogram convolutional model, which can achieve 96.40% accuracy with the least amount of complexity and training time, is the best model for classification, according to experimental data [14]. Chiba's group proposed a microwave and millimeter-wave photonics-based RF signal estimation scheme that utilizes two parallel optical phase modulations of interfering signals and low-pass optical direct detection to convert the complex amplitudes of RF signals into interfered light waves. Experiments revealed that the scheme can successfully evaluate 10 GHz RF signals from 20 kHz oscillating signals obtained by direct detection [15]. The summary table for related work is shown in Table 1.

Table 1: Summary table for related works

Researchers	Method	Accuracy (%)	Processing Time (s)	Robustness to Noise
Zhai et al	High-voltage power supply EMN filtering	93.2	21	Moderate
Han et al	Dual-frequency asymmetric transmission supersurface	94.6	34	High
Li et al	Magnetelluric noise suppression method	92.7	24	Moderate
Wang et al	radar transmit matri	97.4	27	High
Zhang et al	Suppress residual self-interference	91.5	24	High
Tan et al	Mitigate the effects of sensor noise	97.5	18	Moderate
Cutts et al	Temporal filtering of RF signals	91.4	37	High
Shi et al	Photonic method for incorporating RF self-interference cancellation	93.7	19	Moderate

Shen et al	A deep learning-based RFFR scheme	96.4	22	High
Chiba et al	A microwave and millimeter-wave photonics-based RF signal estimation scheme	93.7	39	High

In summary, many researchers have conducted studies for EMN interference signal processing and RF identification techniques. However, these researches still have limitations such as RFFR error, bandwidth limitation and so on. Therefore, the study proposes the RFFR technique considering EMN strong interference and expects to provide a more effective RFFR method.

2 Design of radio frequency fingerprint recognition methodology

This chapter focuses on the design of the RFFR method, including the RF signal processing method for EMN strong interference and the residual network (ResNet) with channel attention mechanism (RN-CAM) model. The first section of this chapter utilizes a deep neural network for feature abstraction and discrimination of raw RF signals, and the second section of this chapter determines the shape and size of the dynamically determined network by means of an adaptive approach in order to achieve the real-time requirements of the RF transmitting source device labeling function.

2.1 Radio frequency signal processing considering strong interference from electromagnetic noise

The electromagnetic environment is complex and variable, and there often exists a large number of redundant signals and irrelevant information, which consume a large amount of storage space and computational overhead, and can affect the real-time performance of the system [16]. Therefore, the study addresses the problem of cleaning and labeling processing of raw signal data in RFFR systems, and proposes a recognition model based on deep neural networks, which directly utilizes the raw sampled RF signals for feature abstraction and discrimination. In parallel, the high-frequency signals are targeted appropriately to determine the signal frequency band of interest. Subsequently, signal tracking and prediction are performed to determine the key signals' corresponding frequency band. Lastly, the training set is built for the purpose of training and testing the recognition model. Furthermore, the LWP procedure for signals is suggested, which entails high-frequency sub-signal screening, targeted signal prediction, and identifying the transmitter source device of the signal in order to enhance the system's accuracy and real-time performance. Figure 1 depicts the LWP process for RF signals.

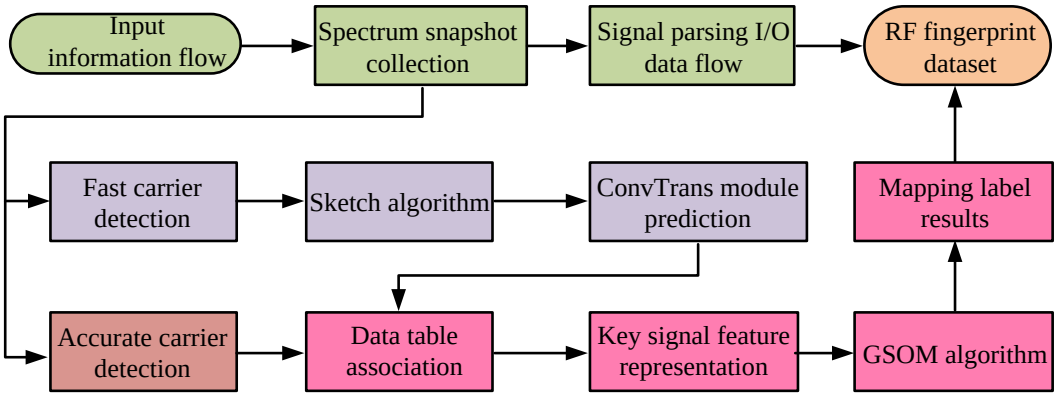

Figure 1: RF signal lightweight process

The two main processes in RF signal LWP are pattern recognition and feature extraction. The enhanced sketch algorithm is initially used to screen the original data in order to identify high-frequency signals for the feature extraction stage. The improved sketch algorithm mainly includes the following steps: 1) The raw data is processed into blocks, with each block comprising a small amount of data. This approach improves computational efficiency. 2) For each small block, the local correlation and remove data points with low correlation is calculated. 3) The aggregation of the filtered data is necessary to obtain high-frequency signals. 4) It is recommended that the aggregation results be arranged in frequency order, with the objective of highlighting the most significant features.

Then, the focus signals resident in the frequency domain are found using a time series prediction network and their feature attributes are extracted, including the center frequency and bandwidth of the focus signals. Finally, the annotations of the key signal transmitting devices are obtained by growth self-organizing model (GSOM) clustering algorithm. In the pattern recognition step, the labeling results are correlated with the I/Q data of the signal segments to obtain the I/Q dataset of the RFFR at the transmitter end [17]. The specific operations include the rapid identification of carriers, the processing of IF signals, the precise detection of carrier features, and the identification of key signals resident in the frequency domain through the sketch-improved algorithm and a time series prediction network. Ultimately, the GSOM clustering algorithm is employed to annotate key signal transmitting devices. The improved sketch algorithm uses self-incrementing identifiers and differentiation rules for signal segments to prevent signal segments with smaller frequency widths from being merged to ensure the statistical accuracy of the algorithm. The specific process includes regularizing the current arriving signals, updating the mapping, clearing the recorded signals that have not been updated for a long time, maintaining the Top-K table and determining whether the table needs to be updated. On this basis, the study proposes a transformer-based convolutional multi-headed self-attention (ConvTrans) temporal prediction network module for analyzing high-frequency sub-signals in terms of the time dimension of outgoing connections and predicting the outgoing trend of the signals in the coming period. In order to further narrow down the range of high-frequency sub-signals to focus on, the module incorporates the attention mechanism (AM). Simultaneously, the outgoing state sequence must be extracted and the time point sequence must be transformed into period sequence in order to satisfy the time series prediction requirements. The focus signal $signal^{i}_{imp}$ is defined as shown in equation (1).

$$signal^{i}_{imp} = \left\{ signal^{i}_{h\_feq} \frac{1}{N} \sum_{k=i+1}^{N} \frac{\sum_{|W|} ducy(signal^{i}_{h\_feq})}{W} \right\} \tag{1}$$

In equation (1), the number of time series is N, the high-frequency signal is $signal^{i}_{h\_feq}$, and the time it is high in a time window W is $ducy(signal^{i}_{h\_feq})$, as shown in equation (2).

$$ducy(signal^{i}_{h\_feq}) = \frac{\sum split(signal^{i}_{h\_feq}, M)}{M} \tag{2}$$

In equation (2), the signal $signal^{i}_{h\_feq}$ is grouped and summed according to M time points result in $\sum split(signal^{i}_{h\_feq}, M)$. The study divides the sequence into corresponding segments through the extraction of high-frequency sub-signal relations and timestamp indexing and generates a one-dimensional feature map by using 1D convolution to causally convolve the sequence and generate a one-dimensional feature map to introduce contextual links in the sequence segments. The ConvTrans input process, the positional encoding PE formula is shown in equation (3).

$$PE(pos, j) = \begin{cases} \sin\left(\dfrac{pos}{10000^{\frac{2j}{W}}} \right), j = 2k \\ \cos\left(\dfrac{pos}{10000^{\frac{2j}{W}}} \right), j = 2k+1 \end{cases} \tag{3}$$

In equation (3), the position of sequence fragment j in the input sequence is pos. The ConvTrans preprocessing and the processing of the input layer are shown in Figure 2.

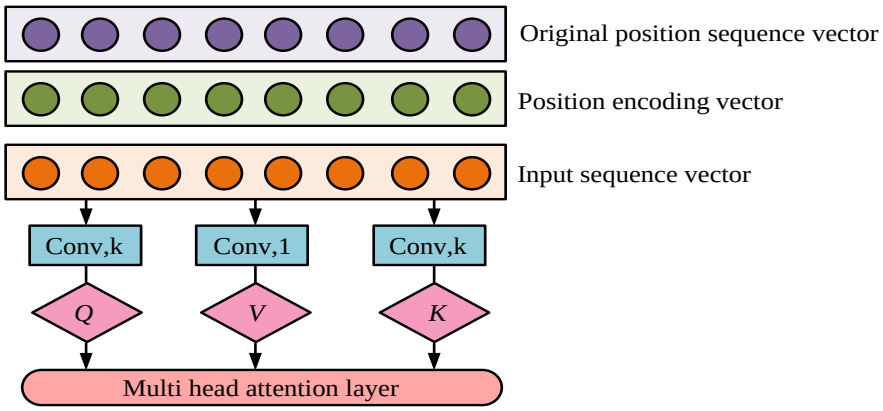

Figure 2: Topic information extraction process

The Transformer EMN utilizes a multi-head self-EMN to capture long and short-term dependent features in a time series and uses multiple attention heads to focus on different aspects of sequence dependent features [18]. The mechanism implements attention by scaling the dot product so that the model focuses on the most relevant elements in a long sequence. Multiple heads of attention $Attention(Q,K,V)$ are computed as shown in equation (4).

$$Attention(Q,K,V) = Softmax\left(\frac{QK^T}{\sqrt{d_k}}\right)V \quad (4)$$

In equation (4), the computed value of the feature vector is V, the input element is K, and its dimension is d_k. the query vector is Q, and the activation function is $Softmax$. The paper suggests a method for determining the size and form of the dynamic determination network based on the adaptive approach, i.e., the GSOM clustering algorithm, in order to satisfy the real-time needs of the annotation function of the RF signal transmitting source device. The GSOM algorithm employs a suppressive mechanism to correct competing neurons that reach the proximity threshold. This mechanism involves reducing the number of neighboring nodes in the neighbor set, thereby achieving a superior clustering effect while minimizing the resource overhead. At the same time, the GSOM algorithm is also able to grow dynamically and adaptively the number of RF transmitters communicating at the current center frequency of the focus signal. The flow of the GSOM algorithm is shown in Figure 3.

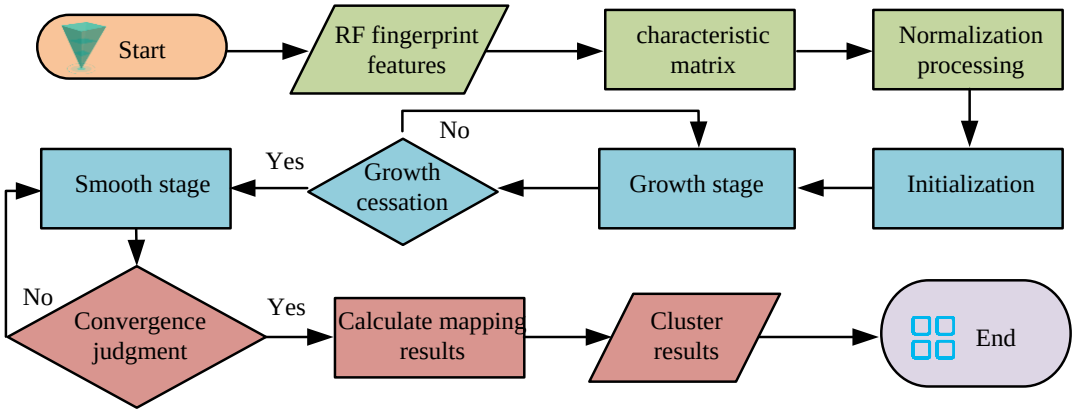

Figure 3: GSOM algorithm process

The GSOM algorithm consists of three phases: initialization, growth and smoothing correction. In the initialization phase, the competing layers contain four initial neurons and the weight vectors are initialized using random values and normalized. In the growth phase, the neuron weights are iteratively updated according to a method similar to the basic SOM. In the smoothing correction phase, the network performs neuron weight updates at a low learning rate, while the learning rate decay rate is gradually reduced to avoid large fluctuations in the weight values. The neuron error update process in the growth phase is shown in equation (5).

$$TE_j(t+1) \leftarrow TE_j(t) + \sqrt{\sum_{k=1}^{N}(x_{ik} - \hat{w}_{jk}(t))^2} \quad (5)$$

In equation (5), the neuron errors at moments t and $t+1$ are $TE_j(t)$ and $TE_j(t+1)$, respectively. The input vector is x_i and the winning neuron weight vector is $\hat{w}_j(t)$. The neuron weights are updated as shown in equation (6).

$$w_j(t+1) = \begin{cases} w_j(t) & , j \notin N_{t+1} \\ w_j(t) + \alpha(t) \times d_j(t), & j \in N_{t+1} \end{cases} \quad (6)$$

In equation (6), the learning rate is $\alpha(t)$, the Euclidean distance between the input vector and the neuron weight vector is $d_j(t)$. The domain neuron of the winning neuron in round $t+1$ is N_{t+1}. The growth threshold is updated as shown in equation (7).

$$GT(t+1) = \frac{D \times (1-SF)^2}{1+1/t} \quad (7)$$

In equation (7), the growth threshold at moment $t+1$ is $GT(t+1)$. The dimension of the input vector is D. The iterations is t, and the scaling factor is SF.

2.2 Radio frequency fingerprint recognition model design

Deep learning in RFFR faces challenges such as noise interference, practical environment variability and unbalanced data volume distribution, which easily lead to model overfitting and failure to meet the actual scene requirements [19]. For this reason, in order to improve the performance of the model, the study suggests an RN-CAM based on the channel EMN to extract RF-FPF.

It also introduces a customized nonlinear activation function and dynamic thresholding noise reduction algorithm, builds a dynamic thresholding noise filtering structure by residual cross-layer connection, and uses a focal loss function to address the category imbalance problem. The structure of the RN-CAM model is shown in Figure 4.

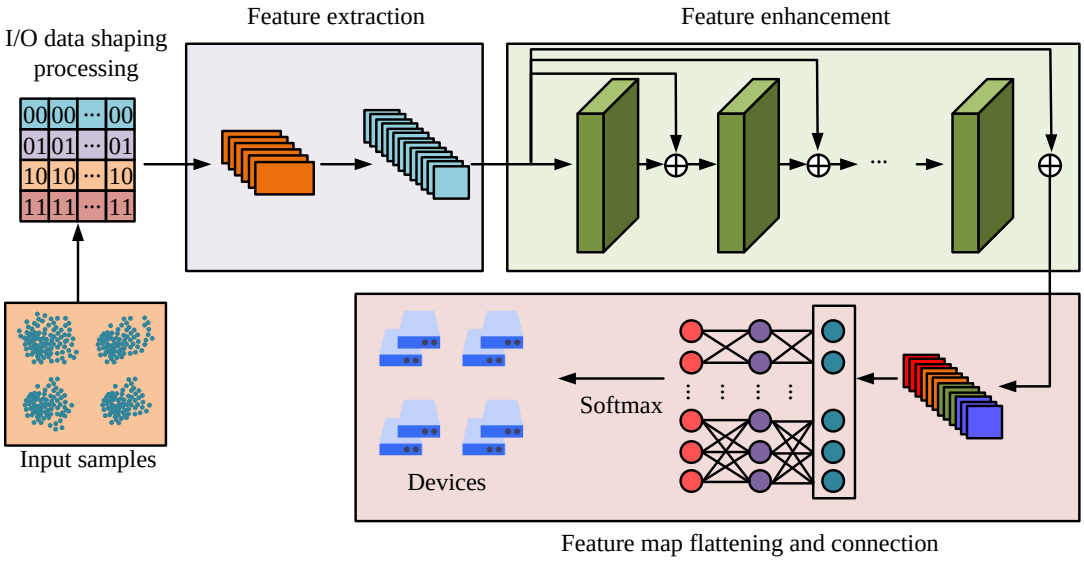

Figure 4: RN-CAM model structure

The RN-CAM model structure employs a two-dimensional convolutional kernel to safeguard the phase feature information of both I/Q data. It also incorporates a channel EMN and a dynamic threshold function. The I/Q data is initially subjected to feature abstraction, after which it is fed into the attention enhancement module. In this module, redundant and irrelevant features in the feature map obtained from the convolutional layer abstraction characterization are set to zero by residual cross-layer connection design, while important features are retained [20]. In essence, a completely linked layer and a Softmax function are employed to ascertain the probability that the RF signal emanates from the device's transmitter. To eliminate text correlation, the I/Q data input to the RN-CAM must be shaped. The I/O modulation signal $s(t)$ is shown in equation (8).

$$s(t)=\cos(2\pi f_0 t)x_i(t)-j\sin(2\pi f_0 t)x_q(t) \quad (8)$$

In equation (8), the baseband signals in the I and Q paths are $x_i(t)$ and $x_q(t)$, respectively, and the fixed carrier frequency is f_0. The baseband signal $\hat{s}(t)$ of the I/O unbalanced modulator is shown in equation (9).

$$\begin{aligned}\hat{s}(t)&=(1+\Delta)\cos(2\pi f_0 t+\theta)x_i(t)\\&-j\sin(2\pi f_0 t))x_q(t)\end{aligned} \quad (9)$$

In equation (9), the imbalance gain of the transmitter is Δ and the imbalance phase is θ. The convolution layer in the RN-CAM network is the key part for extracting the I/signal features, which contains the three operations of convolution, pooling and activation. In order to avoid the loss of RF-FPF information caused by the pooling process, this network discards the pooling process in the convolutional layer. Prior to the attention enhancement module, the 2D convolution works in a way that focuses on single I or Q feature extraction to preserve the independence of the two I/Q paths. In addition, the network employs the PReLU activation function rather than the traditional ReLU in order to maintain the signal phase properties of the I/Q data. PReLU does not set negative input values to zero when dealing with them, but instead deflates them, thus preserving the activation values of negative values. The PReLU activation process is shown in equation (10).

$$PReLU(x_i)=\begin{cases}x_i, x_i>0\\a_i x_i, x<0\end{cases} \quad (10)$$

In equation (10), the trainable parameter is a_i. The attention enhancement module is a key part of the RN-CAM model, which is designed to enhance the potential device FPFs in the I/Q data in the high-intensity EMN acoustic environments. The module mainly includes the RN-CAM weighting value training, dynamic thresholding to suppress the noise, and residual connectivity across layers. During the channel attention weighting value training process, the dynamic threshold is derived from the data noise condition, which converts the valid information into significant features and the noise information into features close to zero. This operation effectively enhances the effective device FPF of the data while suppressing irrelevant information.

Equation (11) displays the dynamic threshold activation function $F(x,t)$.

$$F(x,t)=\text{sgn}(x)\max[(|x|-th),0] \tag{11}$$

In equation (11), the sign function is $\text{sgn}(x)$ and the threshold is th. The RN-CAM combines the spatial entropy network (SENet) and the Inception multibranch network structure to determine the training data noise threshold. The mechanism improves the abstract representation of the network by recalibrating the convolutional feature maps, while suppressing redundant features by introducing the Inception multibranch network structure to extract phase features of the I/Q data. In the RN-CAM, global information can be extracted and learned by global average pooling and selective convolution of the convolutional feature map to improve the accuracy of noise threshold estimation [21]. The structure of the RN-CAM is shown in Figure 5.

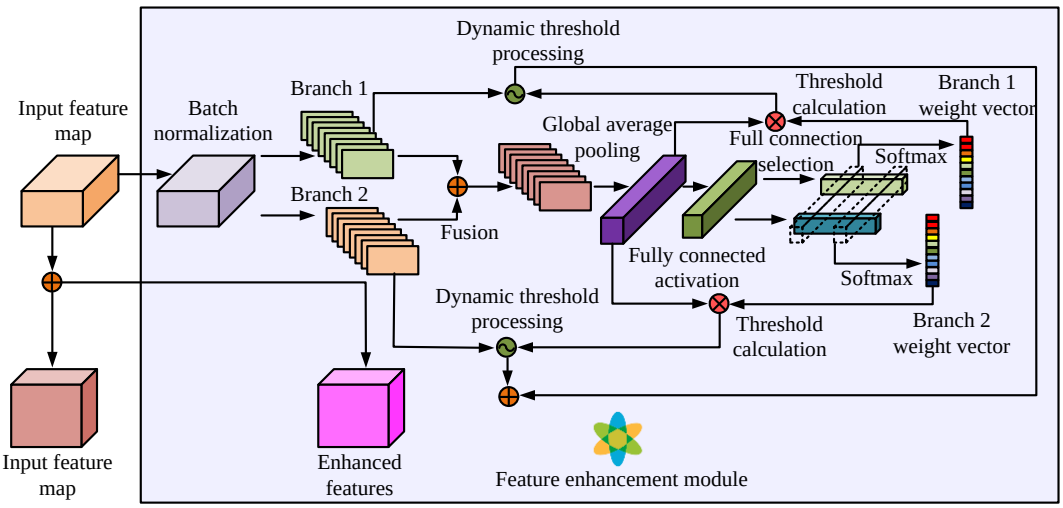

Figure 5: Channel attention mechanism structure

To decrease the difficulty of model training, the input convolutional feature maps need to be batch normalized, and the results of the normalization process are shown in Equation (12).

$$Oy_i=\gamma Ix_i+\beta \tag{12}$$

In equation (12), the input and output tensors in the same batch are Ix_i and Oy_i, respectively, and the trainable parameters are γ and β, respectively. The result of the pass feature compression is shown in equation (13).

$$sc=GAP(U)=\frac{1}{H\times W}\sum_{i=1}^{H}\sum_{j=1}^{W}U(i,j) \tag{13}$$

In equation (13), the feature map is U, the feature compression result is sc, the global average pooling operation is GAP, and the feature map height and width are H and W, respectively. The final feature enhancement result V is shown in equation (14).

$$V=F(U_a,t_a)+F(U_b,t_b) \tag{14}$$

In equation (14), the dynamic thresholds of the branch activation functions are t_a and t_b, and the convolutional feature results of the two branches are U_a and U_b, respectively. The model loss function BB is shown in equation (15).

$$Loss=-\sum_{i=1}^{K_s}\varphi_i(1-p_i)^{\gamma}\log(p_i) \tag{15}$$

In equation (15), the category weight is φ_i and the category probability is p_i. The difficulty weight is γ and the number of sample categories is K_s.

3 Application analysis of radio frequency fingerprint recognition methods

This chapter focuses on validating the sketch algorithm and the RFFR model, respectively, and comparing their performance with other models. This chapter's first section looks at how changing a few of the sketch algorithm's parameters affects signal processing. The second section of this chapter tests the RFFR model using real and simulated datasets and compares it with other models.

3.1 Application analysis of lightweight processing method for radio frequency signals considering strong interference from electromagnetic noise

The experiments are conducted using CentOS 7.4 operating system, Python 3.7 programming language and PyTorch 1.7.1 programming framework, and CUDA 10.1 general-purpose parallel computing architecture. The experiments first evaluate the sketch algorithm, which

mainly optimizes the size of the sketch structure through the configuration of two parameters, width and depth, and the tuning of the parameters using a grid search algorithm. The selection of specific parameter values is intended to optimize the performance of the sketch algorithm and ConvTrans network, reduce statistical errors, improve prediction accuracy, and conserve storage space and processing time. The use of a grid search algorithm to adjust the width and depth of the sketch structure, as well as to optimize the ConvTrans network with the number of times point aggregates and time windows, results in an improved performance of the algorithm in the detection of high-frequency signals, time series prediction, and clustering analysis. Table 1 displays the sketch algorithm's performance.

Table 1: Performance of sketch algorithm

Record quantity	Record size (MB)	Statistical error of high-frequency signals (%)	Statistical error of intermediate frequency signals (%)	Processing time(s)	Sketch structure size (MB)
0.5×105	220	4.8%	11.1%	3.8	1.19
1×105	440	10.1%	16.3%	6.3	
2×105	860	11.6%	15.6%	12.1	
4×105	1640	10.4%	18.3%	24.2	
8×105	3860	12.7%	19.3%	35.3	
12×105	445000	13.7%	19.8%	43.7	

In Table 1, meanwhile, the sketch algorithm is able to control the estimation error of high-frequency sub-signals within 14%, which indicates that the algorithm performs well in the determination of high-frequency sub-signals and the subsequent timing prediction and clustering analysis. The structure size of the sketch algorithm is 1.19 MB after the completion of statistics, which can effectively compress the signal and thus save storage space. In addition, the execution efficiency and processing speed of the sketch algorithm are quite impressive. The processing time of 12×105 records is only 43.7 s, which indicates that the algorithm can meet the real-time demand. After the high-frequency signals are screened, they need to be analyzed and processed through the ConvTrans network. The effect of the number of time-point aggregation and the number of time windows on the ConvTrans network is shown in Figure 6.

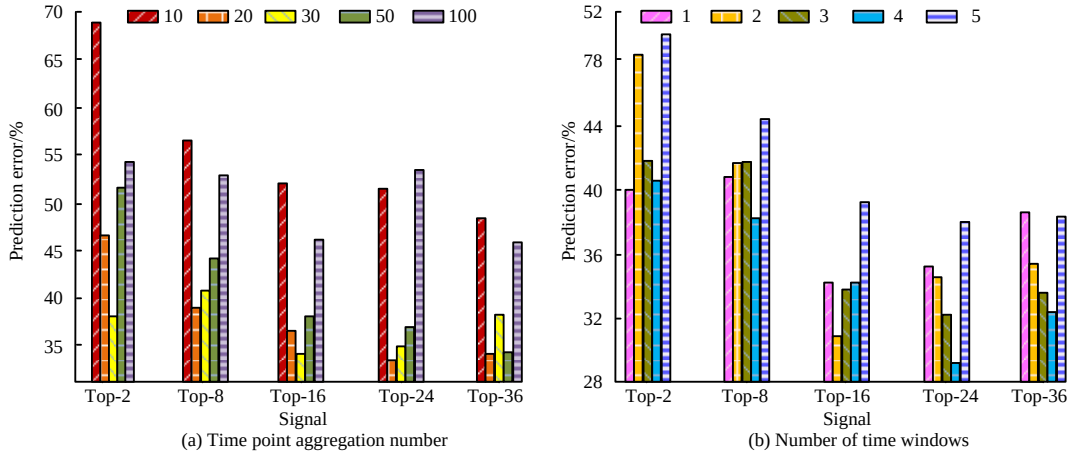

(a) Time point aggregation number (b) Number of time windows

Figure 6: The impact of the number of aggregation points and time windows on the ConvTrans network

The impact of time-point aggregation number on the ConvTrans network is depicted in Figure 6(a). The findings reveal that when the time-point aggregation is 30, the ConvTrans network has the smallest average value of 34.6% in the timing prediction error, which can maximally retain the trend of the signal duty cycle change. However, high-frequency sub-signals with long durations showed larger errors during the prediction process. This is due to the high duty cycle of high-frequency sub-signals in the time domain, which leads to data

sparsity and prevents the model from accurately predicting the pattern of short-term jitter of the sequence. Nonetheless, the prediction results for signals with long durations are still the focal signals. Therefore, the focus of the model in the prediction task should be concentrated on signals with a large span of duration intervals, such as Top-24 and Top-36. The impact of changing the number of time frames on the ConvTrans network is depicted in Figure 6(b). When the number of time windows is 4, the average value of prediction error of ConvTrans network is the smallest, which is 32.8%. The results show that the prediction performance of ConvTrans network is optimal when the number of time point aggregation is 30 and the number of time windows is 4. The experiment uses the recurrent neural network (RNN) model and the long short-term memory (LSTM) model as a comparison in order to further compare and validate the prediction abilities of the ConvTrans network. The comparison of the prediction results of different network models is shown in Figure 7.

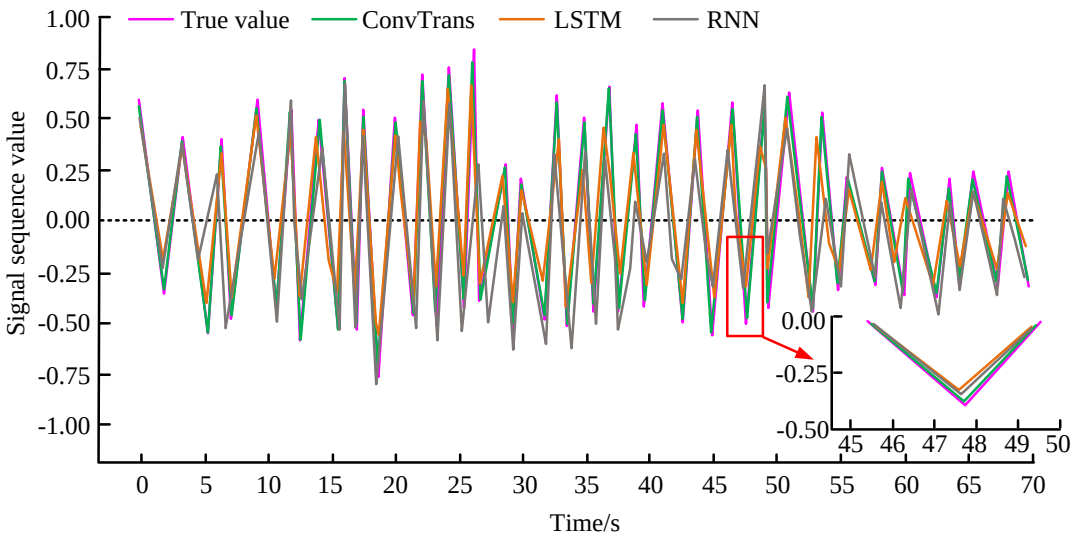

Figure 7: Comparison of prediction results of different network models

Figure 7 shows that the LSTM network model has a prediction error of approximately 21.3%, the RNN network model has a prediction error of approximately 19.8%, and the ConvTrans network model has a prediction error of approximately 12.1%. Among the different network models, the ConvTrans network model predicts the results closest to the true values. In addition, the ConvTrans network model has a lower prediction error compared to the LSTM and RNN network models, which also implies that the model has a higher accuracy in predicting sequence data. In the context of RFFI, ConvTrans networks demonstrate superior performance compared to LSTM and RNN models, largely due to their optimization of the number of times point aggregates and time windows. The experimental results demonstrate that the ConvTrans network exhibits the lowest prediction error under specific conditions and is capable of more accurately capturing key features and trends in sequence data. Furthermore, the ConvTrans network model demonstrates remarkable adaptability to short-term jitter in sequence data, thereby reducing prediction errors. In comparison to LSTM and RNN models, ConvTrans networks exhibit notable advantages in terms of prediction accuracy and performance. Consequently, the ConvTrans network is a more effective prediction method in RFFI. The Euclidean distance between clusters and the average distance from the data to the center of mass within clusters are measured by the Davidson Boulding index (DBI). To gain a better understanding of the relationships between clusters and the distribution of data inside clusters, the mean value of the highest similarity between cluster classes can be computed. The smaller value of DBI indicates that the smaller the difference of data within clusters, the higher the similarity, and the better the clustering effect. The experiment compares the self-organizing model (SOM), density clustering algorithm (DCA), and K-means algorithm in order to confirm the efficacy of the GSOM clustering algorithm suggested in the study. Figure 8 displays the comparison results of various clustering strategies.

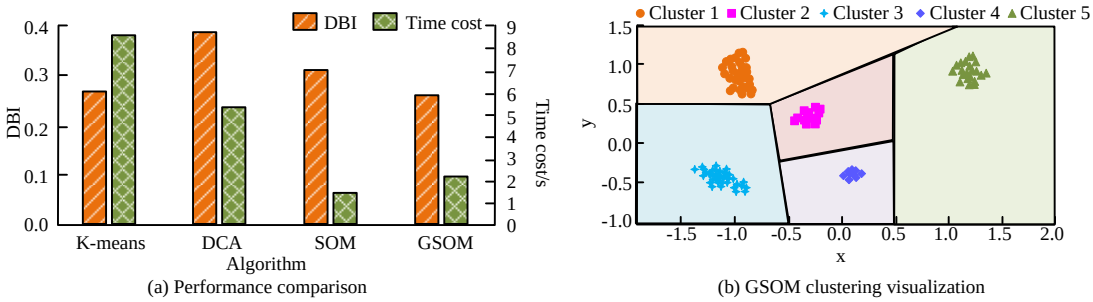

(a) Performance comparison (b) GSOM clustering visualization

Figure 8: Comparison results of different clustering algorithms

Figure 8(a) shows the DBI and time overhead of different clustering methods, and the DBI of K-means, DCA, SOM and GSOM clustering algorithms are 0.2691, 0.3739, 0.3129 and 0.2639, respectively. The time overheads of K-means, DCA, SOM and GSOM clustering algorithms are 8.6s, 5.3s, 1.5s and 2.3 s. The results show that the GSOM clustering algorithm performs well in terms of clustering performance and computational efficiency, and has lower DBI and time overhead compared to other clustering algorithms. The GSOM clustering algorithm's visualization results for signal clustering are displayed in Figure 8(b). The bigger distances between distinct clusters and the smaller distances between the same clusters suggest that the algorithm is effective at signal clustering.

3.2 Application analysis of radio frequency fingerprint recognition model

The implementation of the RN-CAM model is contingent upon the TensorFlow deep learning framework. Prior to the training process, the raw data undergoes preprocessing. Subsequently, the preprocessed data is inputted into the RN-CAM model for training. During the training process, the cross-entropy loss function and Adam optimizer are employed to enhance the convergence velocity and recognition accuracy of the model. Finally, the optimal model parameters and structure are selected based on the results of the validation set, thereby achieving high recognition accuracy. The experiments are carried out to evaluate the model using both real and simulated datasets in order to validate the efficacy of the RFFR model suggested in the study. Table 2 displays the authentic dataset.

Table 2: Real dataset situation

Bandwidth (KHz)	Equipment number	Center frequency point (MHz)	Data volume
25	1	1020	32000
	2	1020	43000
	3	1040	62000
	4	1040	22000
30	1	1040	77000
	2	1040	81000
	3	1060	93000
	4	1060	17000

The experiment used visual geometry group (VGG), ResNet, and deep convolutional neural network (DCNN) as comparative approaches to assess the efficacy of the RN-CAM model. Figure 9 displays the results of a performance comparison between various models.

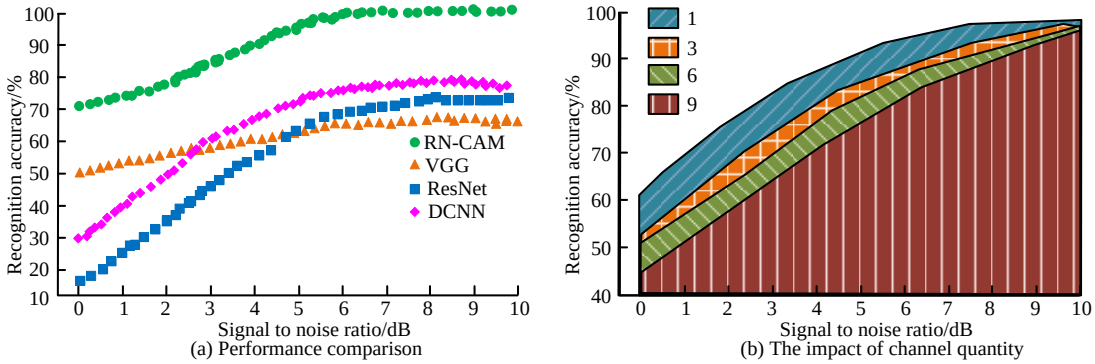

(a) Performance comparison (b) The impact of channel quantity

Figure 9: Performance comparison results of different models

A comparison of the recognition accuracy of several models is presented in Figure 9(a). When the signal-to-noise ratio (SNR) is 10dB, the recognition accuracy of the RN-CAM model, VGG, ResNet, and DCNN are 98.2%, 63.1%, 68.4%, and 72.5%, respectively. The RN-CAM model has the highest recognition accuracy out of the four models, indicating that it is more generalizable in the context of RFID fingerprint recognition tasks. The recognition accuracy of the RN-CAM model with varying numbers of channels is displayed in Figure 9(b). The RN-CAM model's recognition accuracy gap under varying channel counts is less than 5% when the SNR is 10 dB, further demonstrating the model's strong generalization capabilities. Meanwhile, the RN-CAM model adopts an end-to-end CNN structure during training, which can ensure high recognition accuracy while reducing computational complexity. Furthermore, the RN-CAM model incorporates residual connections and pooling operations, which facilitate accelerated calculation. Consequently, while maintaining a high degree of recognition accuracy, the RN-CAM model exhibits commendable computational efficiency. The RN-CAM model is suitable for real-time implementation in RFID fingerprint recognition tasks, primarily due to its lightweight network structure and rapid training convergence. The test results of the RN-CAM model in unbalanced data are shown in Figure 10.

(a) Optimization 1 (b) Optimization 2

Figure 10: Test results of RN-CAM model in imbalanced data

The test results of the RN-CAM model following cross-entropy loss function optimization are displayed in Figure 10(a), and the model's prediction accuracy is greater than 73.7%. The test results of the RN-CAM model following focus loss function optimization are displayed in Figure 10(b), and the model's prediction accuracy is greater than 83.7%. The RN-CAM model performs better on the unbalanced dataset with improved prediction accuracy when the focus loss function is optimized.

4 Discussion

The RFFR method under study exhibits notable advantages in performance when compared to existing advanced technologies. Comparative experiments have

demonstrated that the proposed RN-CAM model exhibits excellent performance in terms of recognition accuracy, processing speed, and computational efficiency. In terms of recognition accuracy, the RN-CAM model achieved a recognition accuracy of 98.2%, which is significantly higher than the 63.1%, 68.4%, and 72.5% of comparative models such as VGG, ResNet, and DCNN. This indicated that the RN-CAM model exhibits superior generalization capabilities in RFFR tasks. Moreover, when the SNR was 10 dB, the recognition accuracy difference of the RN-CAM model under different channel numbers was less than 5%, thereby further substantiating the consistency of the model's performance under varying conditions. In terms of processing speed and computational efficiency, the RN-CAM model exhibited high efficiency in processing large amounts of data. In comparison to existing advanced methods, the RN-CAM model demonstrated notable advantages in data compression and storage space. The existing methods required a sketch structure size of 1.19 MB under the same conditions, while the RN-CAM model reduces this value to approximately 0.26 MB, effectively reducing the storage space requirements. The RN-CAM model employs an end-to-end recognition framework based on CNNs, which effectively extract signal features and enhance recognition accuracy. The incorporation of a self-AM within the network enables the model to capture time-varying information and frequency differences in the signal, thereby enhancing its generalization ability. The model's performance is enhanced by the adoption of a strategy of balancing data, which enables it to handle imbalanced datasets more effectively. Nevertheless, while RN-CAM models enhance performance, they also exhibit certain limitations. In environments with a high level of EMN interference, the model may be affected to some extent, resulting in a decrease in recognition performance. Furthermore, the RN-CAM model exhibits relatively high prediction errors when processing high-frequency sub-signals with long durations. This phenomenon is primarily attributable to the high duty cycle of high-frequency sub-signals in the time domain, which results in sparse data and consequently impairs the prediction accuracy of the model.

5 Conclusion

To suppress noise interference and reduce data redundancy, the study employs ResNet and CAM for feature extraction and clustering analysis of RF signals, with the objective of facilitating the identification of fingerprints. The experimental results indicated that the ConvTrans network minimized the average value of temporal prediction error when the number of time points aggregation was 30. When the number of time windows was 4, the ConvTrans network had the lowest average prediction error. The DBIs for the K-means, DCA, SOM, and GSOM clustering algorithms were 0.2691, 0.3739, 0.3129, and 0.2639, respectively. The time overheads for the K-means, DCA, SOM, and GSOM clustering algorithms were 8.6 s, 5.3 s, 1.5 s, and 2.3 s. The GSOM clustering algorithm had a lower DBI and time overhead compared to the other clustering algorithms. At an SNR of 10 dB, the RN-CAM model achieved the highest recognition accuracy of 98.2%, while VGG, ResNet, and DCNN achieved recognition accuracies of 63.1%, 68.4%, and 72.5%, respectively. The results show that the research method can achieve fast and accurate recognition and classification of RF signals, which provides an effective solution for the RFFR technique. The limitations of this study are that the quality of the dataset and the training time of the model still need to be improved. In order to further improve the recognition performance, future research can consider collecting more high-quality datasets and performing more effective model optimization.

References

[1] S. Huang, S. Wang, Y. Sun, and Y. Zhang, “Efficient processing power harmonic noise with fluctuation frequency in urban transient electromagnetic surveys,” Review of Scientific Instruments, vol. 92, no. 4, pp. 44501-44505, 2021. https://doi.org/10.1063/5.0040092

[2] S. C. Shekar, W. Zhao, T. K. Weldeghiorghis, and T. Wang, “Effect of cross polarization radiofrequency phases on signal phase,” Solid State Nuclear Magnetic Resonance, vol. 117, no. 1, pp. 101771-101776, 2022. https://doi.org/10.1016/j.ssnmr.2021.101771

[3] Y. Guo, and L. D. Yang, “LFM signal optimization time-fractional-frequency analysis: Principles, method and application,” Digital Signal Processing, vol. 126, no. 1, pp. 103505-103518, 2022. https://doi.org/10.1016/j.dsp.2022.103505

[4] Y. Wakisaka, D. Iida, H. Oshida, and N. Honda, “Fading suppression of Φ-OTDR with the new signal processing methodology of complex vectors across time and frequency domains,” Journal of Lightwave Technology, vol. 39, no. 13, pp. 4279-4293, 2021. https://doi.org/10.1109/JLT.2021.3071159

[5] H. Wei, T. Qi, G. Feng, and H. Jiang, “Comparative research on noise reduction of transient electromagnetic signals based on empirical mode decomposition and variational mode decomposition,” Radio Science, vol. 56, no. 10, pp. 64-82, 2021. https://doi.org/10.1029/2020RS007135

[6] L. Zhai, G. Hu, C. Song, M. Lv, and X. Zhang, “Comparison of two filter design methods for conducted EMI suppression of PMSM drive system for electric vehicle,” IEEE Transactions on Vehicular Technology, vol. 70, no. 7, pp. 6472-6484, 2021. https://doi.org/10.1109/TVT.2021.3080924

[7] J. Han, and R. Chen, “Dual-band metasurface for broadband asymmetric transmission with high

efficiency," Journal of Applied Physics, vol. 130, no. 3, pp. 34503-34510, 2021. https://doi.org/10.1063/5.0056700

[8] X. T. J. Li, "Noise suppression for magnetotelluric using variational mode decomposition and detrended fluctuation analysis," Journal of Applied Geophysics, vol. 180, no. 1, pp. 104127-104139, 2020. https://doi.org/10.1016/j.jappgeo.2020.104127

[9] S. Wang, Z. Liu, R. Xie, L. Ran, and J. Wang, "MIMO radar waveform design for target detection in the presence of interference," Digital Signal Processing, vol. 114, no. 5, pp. 103060-103068, 2021. https://doi.org/10.1016/j.dsp.2021.103060

[10] J. Zhang, M. Ma, J. Ma, M. Zou, and B. Jiao, "Residual self-interference suppression guided resource allocation for full-duplex orthogonal frequency division multiple access system," IET Communications, vol. 14, no. 1, 47-53, 2020. https://doi.org/10.1049/iet-com.2019.0723

[11] J. Tan, H. Wu, K. H. Chow, and S. H. G. Chan, "Implicit multimodal crowdsourcing for joint RF and geomagnetic fingerprinting," IEEE Transactions on Mobile Computing, vol. 22, no. 2, pp. 932-950, 2021. https://doi.org/10.1109/TMC.2021.3088268

[12] S. A. Cutts, F. Joshua, R. F. Betzel, O. Sporns, "Uncovering individual differences in fine-scale dynamics of functional connectivity," Cerebral Cortex, vol. 33, no. 5, pp. 2375-2394, 2022. https://doi.org/10.1093/cercor/bhac214

[13] T. Shi, Y. Chen, and Y. Chen, "Photonic-enabled radio frequency self-interference cancellation incorporated into an in-band full-duplex radio-over-fiber system," Optical Engineering, vol. 61, no. 3, pp. 34108-34119, 2022. https://doi.org/10.1117/1.OE.61.3.034108

[14] G. Shen, J. Zhang, A. Marshall, L. Peng, and X. Wang, "Radio frequency fingerprint identification for LoRa using deep learning," IEEE Journal on Selected Areas in Communications, vol. 39, no. 8, pp. 2604-2616, 2021. https://doi.org/10.1109/JSAC.2021.3087250

[15] A. Chiba, and Y. Sunaga, "Complex amplitude estimation of a monochromatic radio frequency signal using frequency downconversion via direct detection of interfered optical phase-modulation signals," Optics Letters, vol. 46, no. 11, pp. 2646-2649, 2021. https://doi.org/10.1364/OL.426425

[16] N. S. Arshad, M. Abdullah, S. A. Samad, and N. Abdullah, "High-intensity lightning recognition system using Very Low Frequency signal features," Journal of Atmospheric and Solar-Terrestrial Physics, vol. 216, no. 1, pp. 105520-105528, 2021. https://doi.org/10.1016/j.jastp.2020.105520

[17] Z. Chen, C. Cai, T. Zheng, J. Luo, J. Xiong, and X. Wang, "RF-based human activity recognition using signal adapted convolutional neural network," IEEE Transactions on Mobile Computing, vol. 22, no. 1, pp. 487-499, 2021. https://doi.org/10.1109/TMC.2021.3073969

[18] C. J. Swinney, and J. C. Woods, "K-means clustering approach to uas classification via graphical signal representation of radio frequency signals for air traffic early warning," IEEE transactions on intelligent transportation systems, vol. 23, no. 12, pp. 24957-24965, 2022. https://doi.org/10.1109/TITS.2022.3202011

[19] I. Salman, and J. Vomlel, "Learning the structure of Bayesian networks from incomplete data using a mixture model," Informatica, vol. 47, no. 1, pp. 83-96, 2023. https://doi.org/10.31449/inf.v47i1.4497

[20] J. Purohit, and R. Dave, "Leveraging deep learning techniques to obtain efficacious segmentation results," Archives of Advanced Engineering Science, vol. 1, no. 1, pp. 11-26, 2023. https://doi.org/10.47852/bonviewAAES32021220

[21] B. M. O. Fraga, U. B. D. Almeida, R. B. Clécio, H. B. Carlos, G. Paolo, S, Patrick, and P. Marcio, "Deep learning Blazar classification based on multifrequency spectral energy distribution data," Monthly Notices of the Royal Astronomical Society, vol. 505, no. 1, pp. 1268-1279, 2021. https://doi.org/10.48550/arXiv.2012.15340